Increased Rigidity of Eglin c at Acidic pH: Evidence from NMR Spin Relaxation and MD Simulations[†]

Hao Hu,[‡,§] Michael W. Clarkson,[‡,§] Jan Hermans,[‡] and Andrew L. Lee*[,‡,||]

Department of Biochemistry and Biophysics, Division of Medicinal Chemistry and Natural Products, School of Pharmacy, and The Molecular and Cellular Biophysics Training Program, School of Medicine, University of North Carolina at Chapel Hill, Chapel Hill, North Carolina 27599

Received June 13, 2003; Revised Manuscript Received September 3, 2003

ABSTRACT: To gain physical insights into how proteins respond to changes in pH, the picosecond to nanosecond time scale dynamics of the small serine protease inhibitor eglin c have been studied by NMR spin relaxation experiments and MD simulations under two pH solution conditions, pH 7 and 3. Like many proteins, eglin c is destabilized by a lowering of the pH, although it retains enough stability to maintain its native conformation at pH 3. Backbone ^{15}N relaxation results show comparable global tumbling times (τ_m) and model-free order parameters (S^2) under the two pH conditions, indicating that the molecule maintains its overall molecular shape and structure at low pH, although the backbone rigidity is slightly increased ($\langle \Delta S_{pH3-pH7}^2 \rangle / \langle S^2 \rangle = 0.6\%$). In contrast, the side-chain methyl dynamics, as measured from ^{2}H relaxation experiments, show a substantial increase in rigidity at lower pH ($\langle \Delta S_{axis,pH3-pH7}^2 \rangle / \langle S_{axis}^2 \rangle = 14.8\%$). Molecular dynamics simulations performed at these pH states produce results consistent with NMR measurements, showing that the two methods are in qualitative agreement. Although a full accounting of the physical basis for the concurrent conformational rigidification and destabilization at low pH requires further investigation, the high level of detail in the MD simulations provides a potential molecular mechanism: the breaking of the hydrogen bond between the side chains of Asp46 and Arg53, and changes in electrostatic interactions, appear to allow the binding loop to move closer to the core part of the protein, resulting in a more compact structure at low pH. This more compact structure may be responsible for the increased level of restriction of molecular motion. As these findings show, the stability of a molecular structure is distinct from its conformational rigidity, and the two can even change in opposite directions, against naïve expectation.

How energetic, structural, and dynamic properties of proteins respond to environmental change is a long-standing question in structural biology (*1*−*6*). As the simplest perturbation to protein structure, the effect of proton binding on the stability and structure of proteins has been widely studied. Destabilization by pH differs from chemical or heat destabilization in that protons bind (or dissociate) and perturb individual side chains, analogous to mutations, which makes the study of the effects of environmental pH uniquely significant to protein structure, dynamics, and energetics. Changes in pH away from native conditions tend to destabilize the native structure; this behavior is well-understood in terms of weakening or disruption of hydrogen bonds and salt bridges and an overall net repulsion between like-charged ionizable side chains. Such behavior is observed with the "acid molten globule" state (*7*). Accordingly, it is commonly assumed that proteins will adopt more flexible conformations under destabilizing pH conditions and, more generally, that destabilized proteins are more flexible. Such generalizations can be difficult to make, as the precise behavior depends on the specific protein. Indeed, the validity in assuming that increased flexibility results from protein destabilization has been called into question recently (*8*) and remains uncertain. Furthermore, given the complexity of protein flexibility, the number of studies aimed at understanding how pH affects the dynamical properties of proteins is relatively low (*9*−*16*). "Flexibility" in proteins encompasses conformational changes occurring on the picosecond time scale up to minutes or hours, and all time scales ought to be taken into account in any discussions of flexibility, whenever possible. Herein, we report a quantitative, site specific analysis of the effect of lowered pH on a model protein's picosecond to nanosecond flexibility using NMR[1] spectroscopy and molecular dynamics simulations.

[†] This work is supported by a research grant (to J.H.) from the National Center for Research Resources, U.S. National Institutes of Health (RR08012), and a grant (to A.L.L.) from the Pharmacy Foundation of North Carolina. H.H. and M.W.C. are supported by the Molecular and Cellular Biophysics Training Program.

* To whom correspondence should be addressed. E-mail, drewlee@unc.edu; fax, (919) 843-5150.

[‡] Department of Biochemistry and Biophysics.

[§] The Molecular and Cellular Biophysics Training Program, School of Medicine.

[||] Division of Medicinal Chemistry and Natural Products, School of Pharmacy.

[1] Abbreviations: NMR, nuclear magnetic resonance; MD, molecular dynamics; rms, root-mean-square; T_1, longitudinal spin relaxation time constant; T_2, transverse spin relaxation time constant; {^{1}H}−^{15}N NOE, heteronuclear nuclear Overhauser effect; S^2, model-free generalized order parameter; S_{axis}^2, order parameter corresponding to the methyl symmetry axis; SAS, solvent accessible surface; GdnHCl, guanidinium hydrochloride; $\langle x \rangle$, mathematical mean value of x.

10.1021/bi035015z CCC: $25.00
Published on Web 11/04/2003

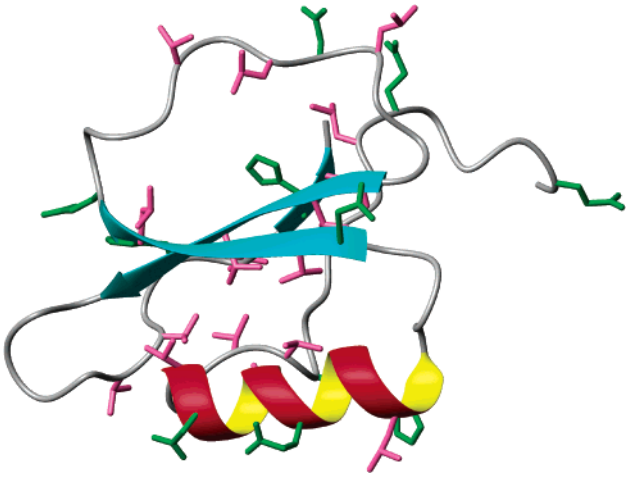

FIGURE 1: Ribbon cartoon representation of the structure of eglin c. The side chains of titratable residues are rendered in green; the side chains of residues Ala, Leu, and Val, which contain methyl groups, are rendered in pink.

NMR spin relaxation provides a sensitive tool for studying protein dynamics. Conventional ^{15}N spin relaxation studies provide dynamics information about the protein backbone on the picosecond to nanosecond time scale (*17*), as well as the microsecond to millisecond time scale using transverse relaxation methods (*18*). ^{13}C and ^{2}H methods allow NMR dynamics studies to extend to the side chains (*19*−*21*). Still, the information obtained from NMR relaxation studies consists of ensemble-averaged properties that fall short of providing full atomic detail. Molecular mechanics-based simulations can characterize dynamics on the picosecond to nanosecond time scale, providing explicit structural and dynamic information at the atomic, or microscopic, level. These two methods are complementary, and their combination has proven to be successful in gaining an understanding of the dynamics properties of various protein systems (*22*, *23*).

To gain physical insight into how pH alters protein dynamics and thermodynamics, we have carried out experimental and theoretical studies on the pH stability and picosecond to nanosecond dynamics of the native state of eglin c, focusing on two pH conditions, pH 7 and 3. Eglin c, a 70-residue serine protease inhibitor from the leech *Hirudo medicinalis*, is soluble and stable over broad pH and temperature ranges, and it contains no disulfide bonds (*24*). It contains a semiflexible binding (or "reactive site") loop, spanning residues 39−49, that interacts with the active site of a subset of serine proteases. X-ray crystallographic (*25*, *26*) and solution structures (*27*) have shown that eglin c adopts the same overall conformation at pH 3 and at neutral pH values, whether in the free form or complexed with serine proteases. The folding and unfolding of eglin c undergo a reversible two-state transition (*28*). The backbone dynamics of wild-type eglin c have been previously reported at pH 3 (*29*, *30*). The structure of eglin c is shown in Figure 1, with the side chains of titratable (affected by acidic titration) and methyl-containing residues (observed in NMR) highlighted.

Like the stabilities of most proteins, the stability (ΔG_{unf}) of eglin c is reduced as the pH is acidified such that at pH 3 it is marginally stable at 2.1 kcal/mol, yet it remains highly structured and globular (*27*, *29*, *30*). ^{15}N spin relaxation experiments at pH 3 and 7 reveal similar backbone dynamics, which indicate subtle, if not negligible, differences between the overall structure and backbone dynamics at the two pH states. However, while protein stability decreases and backbone dynamics are largely unaffected, side-chain rigidity *increases* at lower pH, as demonstrated by the substantial increase in model-free order parameters of side-chain methyl groups (S_{axis}^2). This may seem counterintuitive, but the effect is reproduced in the MD simulations. Analysis of the MD simulations has allowed a simple molecular mechanism to be postulated here. The novel observations made here should contribute to a better understanding of the coupling among structure, dynamics, and energetics in proteins.

MATERIALS AND METHODS

Protein Expression and Purification. Eglin c, containing an F → W mutation at position 10, was used in place of wild-type eglin c in all experiments. This mutation was made for the purpose of fluorescence detection and has a negligible effect on stability (*31*) and dynamics (unpublished data). The protein was expressed using a pET28a plasmid (Novagen) in *Escherichia coli* BL21(DE3). Uniform labeling with ^{15}N (^{13}C) was accomplished by growing cells in M9 minimal medium containing $^{15}NH_4Cl$ ([U-^{13}C]-D-glucose) as the sole nitrogen (carbon) source. Medium was prepared using 60% D_2O when fractional ^{2}H labeling was required.

Cells were grown to an OD_{600} of ∼0.6 and induced with IPTG for 4 h at a final concentration of 2 mg/L of medium. Cells were then pelleted by centrifugation and subjected to three rounds of freezing and thawing. Following resuspension of the pellet in 20 mM Tris-HCl (pH 8.0) and sonication, the suspension was centrifuged at 6000*g* for 30 min. The supernatant was treated with 0.2% polyethyleneimine followed by another round of centrifugation at 23000*g* for 15 min. Lysates were dialyzed overnight against 20 mM Tris-HCl (pH 8.0) and 20 mM NaCl, passed over a Q-Sepharose column (Pharmacia), and eluted with a salt gradient. The eluate was concentrated using a pressure ultrafiltration unit (Amicon) and then passed over a G-50 Sephadex column (Pharmacia). Eglin c purity was assessed by SDS−PAGE. The pure protein solution was concentrated and dialyzed against NMR buffer [20 mM K_2HPO_4 (pH 3.0 or 7.0), 50 mM KCl, and 0.02% NaN_3]. The final concentration of eglin c in samples for relaxation studies was 1.7−2.0 mM, dissolved in 10% D_2O NMR buffer.

Free Energy of Unfolding. The unfolding free energy of eglin c (F10W) was determined by GdnHCl-induced chemical denaturation. Denaturation of eglin c was monitored by tryptophan fluorescence using an ATF105 Dual Channel Titrating Fluorometer (Protein Solutions, Inc.) (*32*, *33*).

In each titration, 1.8 mL of the initial protein sample without GdnHCl was placed in a cuvette (kept in a jacketed cell holder with a thermostat, a thermoelectric heater, with a circulated water cooling system and stirred using a magnetic stirring apparatus) and then titrated with a 7.3 M GdnHCl solution with the same protein concentration used in the initial protein sample, both prepared at the desired pH in appropriate buffers. Titrations were performed at 0.2 M GdnHCl intervals in the ranges of 0−1.2 and 4.5−6.0 M, and at 0.1 M GdnHCl intervals from 1.2 to 4.5 M. The intrinsic fluorescence of each sample was measured by exciting the samples at 290 nm and monitoring emission at

350 nm. An interval of 30 s was used to allow the protein to reach equilibrium after each change in denaturant concentration (*33*).

Fluorescence intensity was analyzed using a two-state unfolding model with the linear extrapolation method (*34*). These were combined into a six-parameter equation to fit the denaturation curves

$$F_{obs} = \{f_N + s_N c_{GdnHCl} + f_D + s_D c_{GdnHCl} \times \exp[m_{N-D}(c_{GdnHCl} - c_{GdnHCl,1/2})/(RT)]\}/\{1 + \exp[m_{N-D}(c_{GdnHCl} - c_{GdnHCl,1/2})/(RT)]\} \quad (1)$$

where c_{GdnHCl} is the denaturant concentration, $c_{GdnHCl,1/2}$ is the denaturant concentration at the midpoint of the transition, f_N and f_D represent the signals for pure native and denatured protein, respectively, without denaturant (the latter extrapolated), s_N represents the first derivative df_N/dc_{GdnHCl}, and similarly for s_D, and m_{N-D} represents the rate of change of the standard free energy of the transition from N to D with the concentration of denaturant. The free energy of unfolding in the absence of denaturant is calculated from

$$\Delta G_{N-D}^{\circ} = -m_{N-D}(c_{GdnHCl} - c_{GdnHCl,1/2}) \quad (2)$$

NMR Spectroscopy. All NMR experiments were performed at 37 °C on either a 500 or 600 MHz Varian INOVA spectrometer equipped with triple-resonance probes and *Z*-axis pulsed-field gradients. NMR data were processed using NMRPipe software for Linux (*35*). Peak assignment and spectral analysis were performed with the assistance of NMRView (*36*) and Sparky (*37*) NMR analysis software.

Assignments of backbone amides and carbon atoms were achieved by gradient-enhanced HNCACB and CBCA(CO)-NH experiments (*38*). Chemical shifts of side-chain carbons and protons were obtained using HCCH-TOCSY (*39*) and $HCCH_3$-TOCSY (*40*) experiments. Stereospecific assignments of prochiral methyl groups were determined using a fractionally ^{13}C-labeled sample (*41*). Titration of acidic side chain groups was monitored using a side chain-optimized version of the HCACO experiment (*42*). The protonation state for the histidine imidazole groups was determined using a two-dimensional (2D) HSQC experiment as a function of pH (*43*, *44*).

^{15}N spin relaxation experiments were performed on samples uniformly labeled with only ^{15}N. ^{2}H spin relaxation experiments were performed on samples uniformly labeled with ^{13}C and randomly fractionally with ^{2}H at the 50−60% level. Relaxation data were collected via a series of HSQC experiments incorporating a variable relaxation delay (*45*). Measurements of ^{15}N T_1 times and $\{^1H\}-^{15}N$ NOEs were obtained as previously described (*45*) with our standard modifications: two high-power, initial ^{1}H saturation pulses (2−4 ms) were inserted at the beginning of the T_1 relaxation delay (*46*). For T_1 experiments, peak intensities corresponding to nine different T_1 delay times (0.037, 0.105, 0.192, 0.296, 0.414, 0.543, 0.685, 0.837, and 1.000 s) were measured, in addition to three duplicated delay times from which experimental uncertainties were estimated. Underlined times indicate repeated experiments for estimating the peak intensity uncertainties. The recycle delay time used in T_1 experiments is no shorter than 1.2 s. Transverse relaxation time constants (i.e., T_2 values) were determined from $T_{1\rho}$ measurements. Delay values used for the experiments were 0.07, 0.017, 0.027, 0.042, 0.062, 0.082, 0.107, and 0.137 s. The observed $T_{1\rho}$ times were corrected for off-resonance T_1 relaxation to yield pure transverse relaxation rates (*47*). ^{15}N spin lock powers that were used were 2.2 and 1.9 kHz for pH 3 and 2.0 and 2.0 kHz for pH 7, at field strengths of 600 and 500 MHz, respectively. To ensure the sample was not overheated during the experiments, recycle delay times in the $T_{1\rho}$ experiments were set to >1.8 s. For all $\{^1H\}-^{15}N$ NOE experiments, ^{1}H irradiation times of 4.5 s were used.

Methyl dynamics information was obtained using deuterium spin relaxation experiments (*19*, *21*) under the same solution conditions that were used in the ^{15}N relaxation experiments. Longitudinal and transverse ^{2}H relaxation rates were determined by observing relaxation of $I_zC_zD_z$ and $I_zC_zD_y$ triple-spin coherences as previously described (*19*). The longitudinal I_zC_z relaxation rate was then subtracted to yield pure D_z and D_y (T_1 and T_2) relaxation rates. Different sets of delay times were used in these experiments: at 500 MHz field, $R(I_zC_zD_z)$, 2.4, 6.8, 12.5, 19.3, 26.9, 35.4, 44.6, 54.4, and 65.0 ms; $R(I_zC_zD_y)$, 1.1, 3.2, 5.8, 8.9, 12.4, 16.3, 20.5, 25.1, and 30.0 ms; $R(I_zC_z)$, 1.0, 9.0, 17.0, 25.0, 33.0, 41.0, 49.0, 57.0, and 65.0 ms; at 600 MHz field, $R(I_zC_zD_z)$, 2.8, 7.9, 14.4, 22.2, 31.1, 40.8, 51.4, 62.8, and 75.0 ms; $R(I_zC_zD_y)$, 1.1, 3.2, 5.8, 8.9, 12.4, 16.3, 20.5, 25.1, and 30.0 ms; $R(I_zC_z)$, 6.0, 14.0, 22.0, 30.0, 38.0, 46.0, 54.0, 62.0, and 70.0 ms. A recycle time of 1.8 s was used in all experiments; 32, 32, and 16 transients/fid were collected for $I_zC_zD_y$, $I_zC_zD_z$, and I_zC_z experiments, respectively, and 47* × 512* points were collected for the $^{13}C(t_1)$ and $^{1}H(t_2)$ dimensions.

The peak intensities from the relaxation experiments (T_1, $T_{1\rho}$, $I_zC_zD_z$, $I_zC_zD_y$, and I_zC_z) were fitted to a monoexponential decay function to yield corresponding relaxation time constants. Peak intensity errors were estimated from the intensity differences between original and duplicate time points. The "model-free" formalism was then used to extract dynamical parameters for various bond vectors (*48*). The overall tumbling time (τ_m) was fitted globally using relaxation data from rigid amides (*49*−*51*). τ_m was then fixed, and S^2 and τ_e parameters were fitted locally using the simple model-free form of the spectral density (*48*). Order parameters were fitted with the program relxn2.1 (*21*), using a grid search/Powell minimization method. Errors were estimated using 150 Monte Carlo simulations for each local fit. Methyl ^{2}H S^2 and τ_e values were fitted using the same τ_m determined from ^{15}N relaxation values. Methyl S^2 values were divided by 0.111 to correct for the reduction in the order parameter caused by the degenerate methyl rotation, yielding the S_{axis}^2 value (*19*, *48*, *52*).

MD Simulations. The program Sigma (*53*) was used for all simulations and analyses, with the charmm22 force field (*54*) for the protein molecule and the TIP3P water model for the solvent (*55*). The NMR structure of wild-type eglin c (PDB entry 1EGL) (*27*) was used as the starting structure. The PDB file contains a collection of 25 structures, of which the first was picked up as the initial model.

Prior to the simulation, several necessary modifications were made to the NMR structure. The side chain of Phe10 was replaced with Trp, to account for the use of the F10W mutant in all experiments. All other side chains were properly protonated in accordance with their pK_a values and the pH intended for simulation. Namely, the side chains of Asp and

Glu are protonated at pH 3 and negatively charged at pH 7; the imidazole groups of three histidine residues are positively charged at pH 3 and neutral at pH 7, where the protonation states have been determined by NMR experiments (*44*). Specifically, the H28 and H68 side chains are protonated at $N^{\epsilon 2}$, and H65 is protonated at $N^{\delta 1}$. The protein molecule was solvated in a cubic box (64 Å × 64 Å × 64 Å) filled with water molecules. The final system contains the protein molecule and 7986 water molecules (~25100 total atoms).

Before the simulation data were collected, the entire system was subjected to a series of equilibration steps. First, the heavy atoms of the protein molecule (except for the side chain of Trp10) were frozen, while the positions of water molecules and hydrogen atoms were changed by energy minimization for 200 steps of the conjugate gradient method, followed by 40 ps of MD simulation at 300 K. Next, the constraints were removed from the side-chain atoms, and the energy of the system was minimized by 100 steps, followed by 200 ps of MD simulation. Finally, all constraints were removed, and the system's energy was minimized for 100 steps. This was followed by 400 ps of MD simulation. The initial temperature of the simulation was 50 K, and this was brought to 300 K over a period of 100 ps.

Except during these equilibration stages, in which time steps of 1 and 4 fs were used for short- and medium-range interactions, respectively, all other simulations employed a multiple-time step scheme (*56*, *57*) with time steps of 2, 6, and 12 fs for short-, medium-, and long-range interactions, respectively. The SHAKE algorithm (*58*) was used to constrain all bond lengths. Ewald summation was used for calculating long-range electrostatic interactions (*59*). The temperature and pressure were restrained by a Berendsen manostat and thermostat (with separate thermostats for solute and solvent), respectively, using relaxation times of 0.1 ps (*60*). For every 12 steps, the nonbond pair list was updated. After every 180 steps, the coordinates of the system were recorded for future analysis. The simulation of the first 2.16 ns was discarded, and only data from the last 43.2 ns simulation period were used.

The calculation of order parameters and correlation times follows approaches published previously by other groups (*61*, *62*). In short, the order parameters S^2 of a bond vector $\vec{\mu}(t)$ is computed as

$$S^2 = \frac{3}{2}[\langle x^2\rangle^2 + \langle y^2\rangle^2 + \langle z^2\rangle^2 + 2\langle xy\rangle^2 + 2\langle xz\rangle^2 + 2\langle yz\rangle^2] - \frac{1}{2} \quad (3)$$

in which x, y, and z are the components of the unit bond vector $\vec{\mu}(t)$ along three Cartesian axes. Here, the braces stand for the ensemble average. Prior to the calculation of S^2, overall translation and rotation of the protein molecule were removed by rigid-body superposition of the structure of the core part of the protein with respect to the experimental NMR structure. We found that inclusion of the loop region in the superposition process essentially does not change the results of the computed order parameters.

The NMR relaxation experiments carried out in this study are limited to motions on the picosecond to nanosecond time scale. Effects from motions longer than the global rotational correlation time generally do not contribute to T_1, T_2, and $\{^1H\}-^{15}N$ NOE, with the exception that slow motions on a time scale of microseconds to seconds will be evident as chemical exchange. Thus, we considered it unwise to use the entire 43.2 ns trajectory over which to calculate order parameters and correlations. Instead, the long trajectory was split into small windows of 2.88 ns each (8000 snapshots). The order parameters and correlation functions were calculated for each window separately, and the results were averaged and the root-mean-square deviations used to estimate a statistical error for the simulation results.

The quasi-harmonic approximation (*63*−*67*) was used to calculate conformational entropy from simulation. This standard method calculates the covariance matrix of the coordinates, and then diagonalizes the covariance matrix to solve eigenvalues of each quasi-harmonic states. The conformational entropy of each state is calculated as a quantum mechanical harmonic oscillator.

Finally, we used the simulation trajectories to compute and compare the compactness of the protein at two pH conditions. The radius of gyration, ρ, of the protein was calculated from

$$\rho^2 = \frac{\sum_{i=1}^{N} m_i(\vec{r}_i - \vec{r}_0)^2}{\sum_{i=1}^{N} m_i} \quad (4)$$

where i represents the N atoms of the protein without N-terminal residues 1−7, m_i the atom's mass, $\vec{r}_i$ its coordinates, and $\vec{r}_0$ the coordinates of the center of mass. The same equation was used to compute, instead of ρ, a mass-weighted root-mean-square distance, D, between the loop atoms and the center of mass of residues 8−70, where now the summations are over all N atoms of the loop region (residues 39−49).

RESULTS

Stability. To assess pH stability, the free energy of unfolding for eglin c was measured over a range of pH values and at two temperatures (Figure 2). All measurements were made on eglin c carrying the F10W mutation (Materials and Methods). The protein is maximally stable at pH ~7, but at pH 3, the stability is reduced to 2.1 kcal/mol at 37 °C. Nonetheless, the protein is predominantly in a single, folded form at both neutral pH and pH 3; this is supported by the appearance of a single set of peaks in the $^{15}N-^1H$ HSQC spectrum recorded at pH 3, corresponding to a single conformation (Figure 3). Under the two-state folding approximation, at pH 3 and 37 °C, the content of unfolded protein is 3% of total protein. This amount of unfolded protein is negligible in the context of these experiments and does not alter the conclusions drawn.

Backbone Dynamics from NMR. Figure 4 shows eglin c ^{15}N relaxation data at pH 7 and 3 at field strengths corresponding to ^1H frequencies of 500 and 600 MHz, respectively. The values of T_1, $T_{1\rho}$, and $\{^1H\}-^{15}N$ NOE are uniform over regions corresponding to the core of the protein. Average T_1 and T_2 times at 600 MHz for all residues are 0.48 and 0.15 s, respectively, at both pH values. The N-terminus and inhibitory binding loop regions, however,

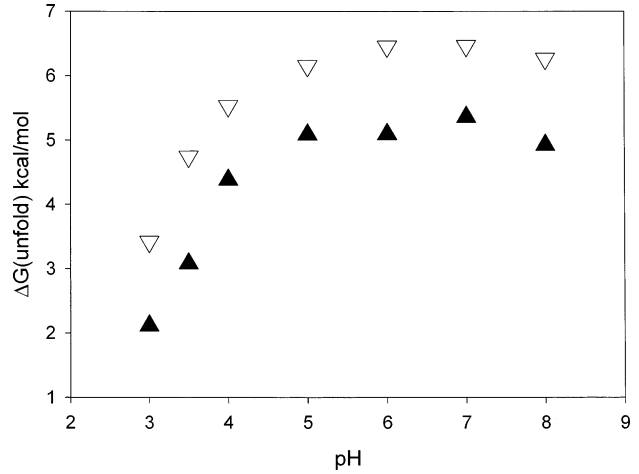

FIGURE 2: Unfolding free energy of eglin c at different pH values determined from fluorescence measurements in the presence of increasing concentrations of guanidine hydrochloride: (▲) 37 and (▽) 25 °C.

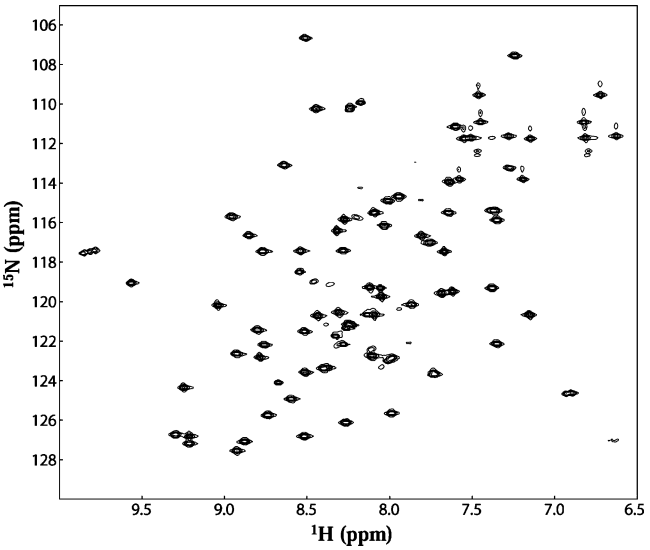

FIGURE 3: ^{15}N−^{1}H HSQC spectrum of eglin c at pH 3 and 37 °C, collected at a ^{1}H frequency of 500 MHz.

show increased relaxation times consistent with increased picosecond to nanosecond motion, as observed previously (*29*, *30*). There are a few peaks (T1, G4, G40, and L45) in the N-terminus and loop region that exhibit line broadening at both pH values, which implies conformational exchange on the microsecond to millisecond time scale. Using the model-free formalism (*17*, *48*, *49*, *52*), the global tumbling correlation time (τ_m) was determined at each pH state. Using these τ_m values, order parameters (S^2) and effective correlation times (τ_e) for individual N−H bond vectors were best-fitted for pH 3 and 7. τ_m was determined to be 4.45 and 4.62 ns at pH 3 and 7, respectively. The observation of comparable values of τ_m indicates that the overall shape and size of the molecule do not change significantly as a result of lowering the pH, consistent with the eglin c structure determined at pH 3 (*27*). The relaxation data were also fitted to a local diffusion model, in which each N−H vector is allowed a local τ_i ($=^1/_6 D_i$) instead of the global tumbling time τ_m (*68*, *69*). We found that the deviations of τ_i from the global τ_m are small. The mean values and rms deviations of the local tumbling times of all N−H bonds of the protein are 4.6 ± 0.2 and 4.4 ± 0.2 ns for pH 7 and 3, respectively. Because of this, as well as because small degrees of anisotropic tumbling have negligible effects on order parameters (*51*), the global tumbling of eglin c was treated as isotropic. The order parameters (S^2) corresponding to backbone N−H vectors calculated from the ^{15}N relaxation data at the two pH values are very similar (Figure 5), although the order parameters at pH 3 show a subtle increase compared to those at pH 7. The mean values of the order parameters of backbone N−H bonds are 0.82 and 0.83 for eglin c at pH 7 and 3, respectively. These ^{15}N relaxation data indicate that lowering the pH does not cause significant changes in the backbone structure or dynamics of the protein.

Side-Chain Dynamics from NMR. Picosecond to nanosecond motions of methyl groups were characterized from relaxation rates of ^{2}H spins in CH_2D isotopomers (*19*). The parameter S_{axis}^2 ($=S^2/0.111$) (*52*) is used to describe reorientational motion of the C−CH_3 bond axis. Typical of most proteins, the methyl S_{axis}^2 values in eglin c are considerably lower and more varied than corresponding backbone NH order parameters (Figures 5 and 6). Whereas the backbone experiences a subtle increase in order parameters ($\langle \Delta S_{pH3-pH7}^2 \rangle = 0.005$ and $\langle \Delta S_{pH3-pH7}^2 \rangle / \langle S^2 \rangle = 0.6\%$), the side-chain methyl axis order parameters (S_{axis}^2) undergo a substantial increase ($\langle \Delta S_{axis,pH3-pH7}^2 \rangle = 0.08$ and $\langle \Delta S_{axis,pH3-pH7}^2 \rangle / \langle S_{axis}^2 \rangle = 14.8\%$) upon lowering the pH from 7.0 to 3.0 (Figure 6). In simple terms, these data indicate that, on the picosecond to nanosecond time scale where side chains exhibit large-amplitude motions (*70*, *71*), eglin c is *more rigid* at pH 3 than at pH 7. This unexpected result appears to contradict the notion that proteins gain flexibility as they are destabilized and underscores the importance of recognizing motions on different time scales (see Discussion).

Backbone Dynamics from MD. As mentioned above, NMR experiments generate ensemble-averaged results lacking microscopic detail. To complement the NMR studies, we carried out separate MD simulations at pH 7 and 3 to enhance the experimental results and to provide structural and dynamical detail that might reveal any sources of the observed dynamical differences. The backbone NH order parameters at the two pH values have been calculated from the respective 43.2 ns trajectories and compared to the NMR-derived results (Figure 1 of the Supporting Information). Except for a few residues at the flexible N-terminus and the loop region, good agreement is observed between experiment and simulation, which is expected for backbone dynamics (*22*, *61*, *62*, *72*−*76*, *89*). General agreement between NMR and MD simulations adds confidence in our use of simulations to provide mechanistic insights into pH-induced rigidification.

Side-Chain Dynamics from MD. A more stringent test of agreement between MD- and NMR-derived dynamics is the comparison of side-chain methyl order parameters, as the side chains have more varied (and less easily predicted) dynamical properties on the picosecond to nanosecond time scale (*70*, *71*). Prediction of side-chain dynamics poses a considerable challenge, requiring an accurate force field and adequate sampling of phase space in the simulations. Analogous to backbone NH groups, side-chain methyl order parameters (S_{axis}^2) were calculated from the two simulations. We have observed a significant overall correlation between side-chain order parameters of eglin c from simulations and experiments (Figure 2 of the Supporting Information). The

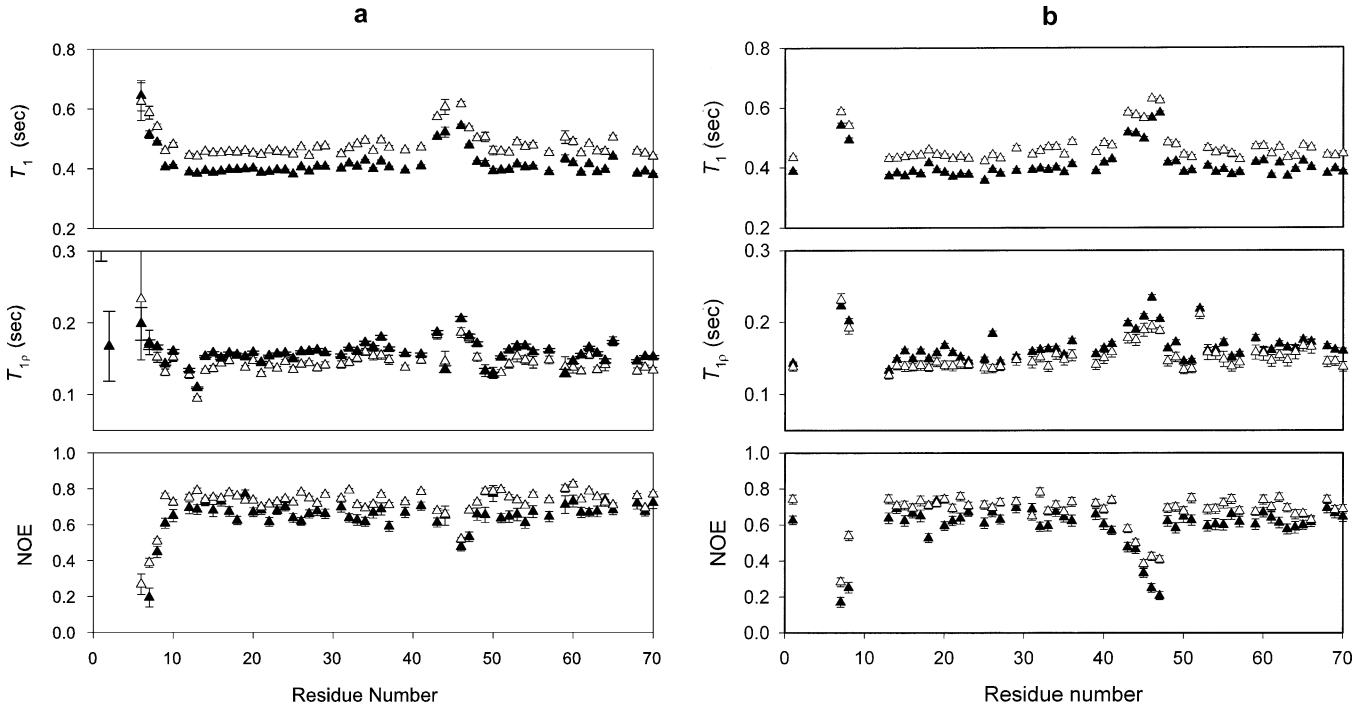

FIGURE 4: ^{15}N spin relaxation data at two different field strengths [(△) 600 and (▲) 500 MHz]: (a) pH 7 and (b) pH 3.

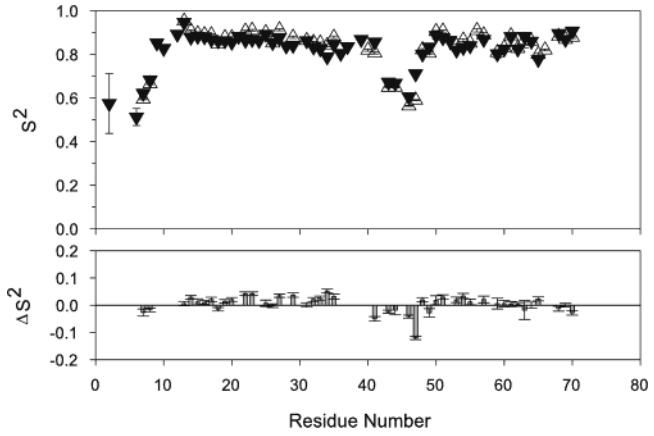

FIGURE 5: NMR-derived model-free order parameters (S^2) for backbone N−H bonds at two pH values. In the top panel, the order parameter is shown as a function of residue number [(▼) pH 7 and (△) pH 3]. In the bottom panel, the difference between the two pH states was computed as $S_{pH3}^2 - S_{pH7}^2$.

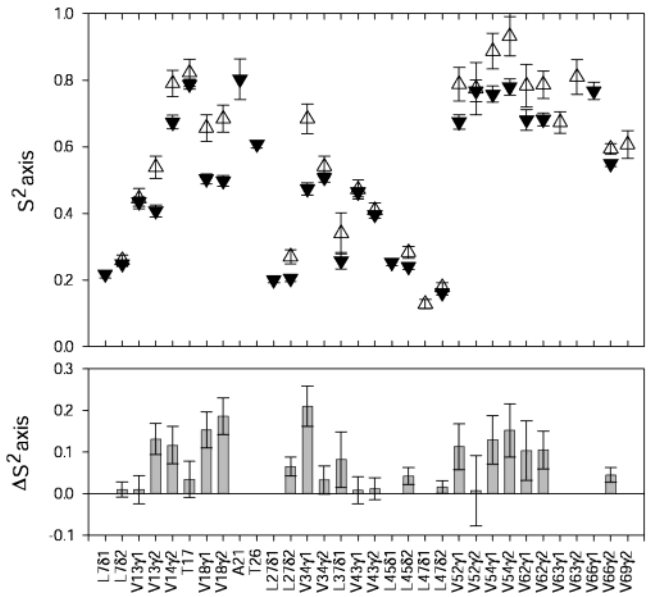

FIGURE 6: NMR-derived model-free order parameters for the side chain methyl groups (S_{axis}^2) at two pH values: (top) order parameter for each methyl group [(▼) pH 7 and (△) pH 3] and (bottom) difference between two pH states computed as $S_{pH3}^2 - S_{pH7}^2$.

pH-induced *changes* in S_{axis}^2 values computed from simulations (results not shown here) correlate less well with the corresponding S_{axis}^2 changes observed by NMR. However, both sets of results show the same overall change in side-chain order parameters, namely, an increase of the average S_{axis}^2 (by 0.012 from the MD value) when the pH is reduced from 7 to 3. Thus, simulations show that the side chains of the protein appear to be more rigid at low pH, in agreement with the NMR results. These observations indicate that, at a qualitative level, the simulations reproduce the experimental results and support the proposition that the protein is more rigid at low pH on the picosecond to nanosecond time scale.

Structural Features. From the solution structure at pH 3 (*27*) and the X-ray structure (bound to subtilisin Carlsberg) at neutral pH (*25*), eglin c exhibits a high degree of structural similarity in its overall topology (C^α rmsd = 0.85 Å for well-defined regions) (*27*). Nonetheless, the free solution structure at pH 3 has measurable deviations from the subtilisin-bound X-ray structure (*27*), evident in the differences in side-chain orientations and some backbone conformations [see discussions on the conformations of P58, G59, and T60 in the reference of Hyberts et al. (*27*)]. To explore subtle structural changes due to the pH change alone, the MD-equilibrated, unbound structures at pH 3 and 7 were compared directly. Prior to this, we compared the MD-equilibrated structures with the experimentally determined structures. At pH 7, we observe several unique features compared to the high-resolution X-ray structure of complexed wild-type protein, crystallized at pH 6.5 (*25*). Most notable structural differences are found in the inhibitory loop. First, instead of a

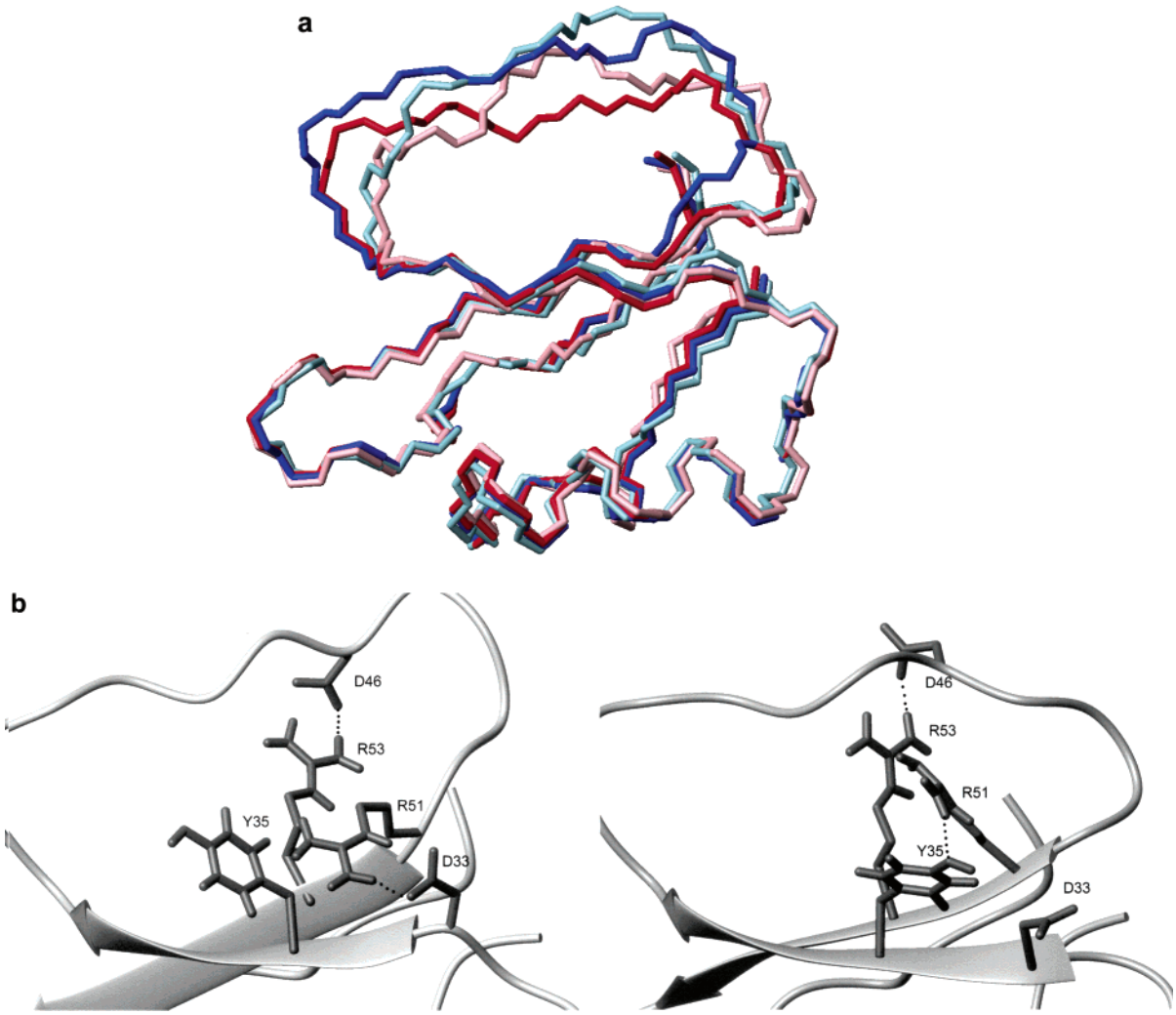

FIGURE 7: Backbone structures of eglin c from simulations. For a clear view, the first seven residues of the N-terminus are not shown. (a) Superposition of simulated mean structures at pH 3 (blue) and pH 7 (red), the NMR structure (first model) determined at pH 3 (light blue), and the X-ray structure determined at neutral pH and complexed with protease (pink). (b) At the left, a snapshot of the simulation at pH 7 shows the H-bonds between D46 and R53 and between D33 and R51, and at the right, a snapshot of the simulation at pH 7 shows the H-bonds between D46 and R53 and between Y35 and R51.

hydrogen bond between the side chains of Arg51 and Asp46, the MD-equilibrated structure has one stable hydrogen bond between the side chains of Arg53 and Asp46 (Figure 7). The side chain of Arg51 shows transient hydrogen bond formation with the side chains of Asp33 or Tyr35, and it switches between these two partners during the simulation (Figure 7b). Such differences are not surprising given that in the X-ray structure, eglin c is complexed with a protease. Our observation is also consistent with the X-ray structure of the uncomplexed protein (*26*), in which no hydrogen bond between Arg51 and Asp46 was reported (coordinates not available). Furthermore, in the X-ray structure of the eglin c complex, the residue at position 33 is Asn, not Asp, which may also account for some of the structural differences.

A comparison between the MD-equilibrated structures at the two pH states shows that the core region conformations are very similar (Figure 7a), with an C^{α} rmsd of 0.35 Å between the two mean structures. They also show the presence, in both, of a hydrogen bond between the side chain of Arg53 and the terminal carboxyl group of Gly70, which is negatively charged at both pH states. As mentioned, at pH 7, the side chain of Arg53 also forms a hydrogen bond with the side chain of Asp46 (Figure 7), while at pH 3, this hydrogen bond is broken due to neutralization, although the two groups remain within a distance consistent with a favorable interaction. At pH 3, the side chains of Arg51 and Arg53 point to directions away from the loop, while at pH 7, the side chain of Arg53 is positioned somewhere between the loop and the central part of the protein, due to the hydrogen bond between Arg53 and Asp46.

Different Compactness of MD-Equilibrated Structures. To investigate the molecular mechanism underlying the apparent rigidification, we have further analyzed the results of the two simulations. A small but systematic difference in the radius of gyration of the protein molecule (calculated with omission of the first seven N-terminal residues) is observed between the two pH states, as shown in Figure 8. The mean values of the radius of gyration are 11.4 and 11.1 Å for eglin c at pH 7 and 3, respectively. Over 95% of the trajectory, the radius of gyration at pH 7 is larger than the mean value at pH 3, and the difference between the mean values exceeds the rmsd of each individual series by a factor of 1.7. This change in the radius of gyration is consistent with the NMR-derived global rotation time (τ_m), which is slightly shorter at pH 3 (4.45 ns) than at pH 7 (4.70 ns).

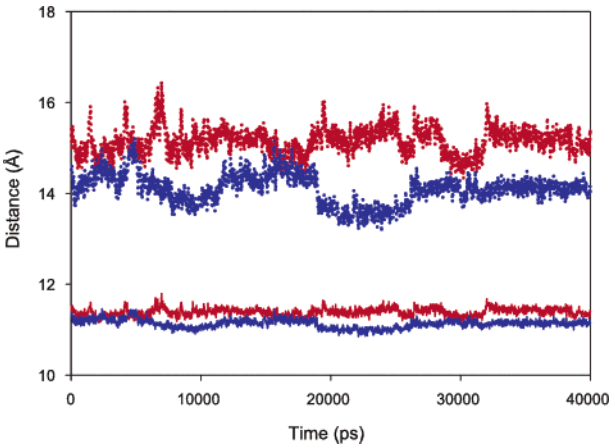

FIGURE 8: Radius of gyration and mass-weighted rms distance between the loop and protein center calculated from simulations: solid lines (bottom), radius of gyration at pH 3 (blue) and pH 7 (red); dotted lines (top), rms distance between the loop and protein center at pH 3 (blue) and pH 7 (red).

As structural changes in the protein core are minimal (Figure 7a), structural changes in the loop region are most likely to explain the changes in the computed radius of gyration. The mass-weighted rms distances between the loop and the center of mass of the central part of the protein (residues 8−70) demonstrate a significant structural alteration for the loop region between pH 3 and 7. The mean values of the mass-weighted rms distances are 15.1 and 14.1 Å for pH 7 and 3, respectively. On average, the loop is closer to the core of the protein at low pH (Figure 8). The reason for this small structural change is the loss of the Arg53−Asp46 hydrogen bond. At pH 7, the side chain of Asp46 points toward the core of the protein, forming a hydrogen bond with Arg53 between the loop and the core, whereas at pH 3, the side chain of Asp46 rotates toward the outside of the protein to interact with solvent; the same behavior is observed with Arg53. This allows the loop to increase its number of interactions with the protein core at pH 3, and the protein is overall more compact than at pH 7. It is important to note that the structural shifts just described are best discussed in terms of time-averaged behavior, as many of these shifts are transient and not captured in all MD snapshots. Transient effects of this kind can be difficult to detect from X-ray diffraction or NMR structural data, and in principle, MD simulations are well-suited to characterization of the transient structural features that contribute to the overall protein characteristics.

A particularly interesting aspect of the overall increase in side-chain order upon acidification is evident from mapping the NMR-observed S_{axis}^2 changes onto the structure of eglin c (Figures 6 and 9). The most significant dynamical changes in methyl-containing residues occur in the hydrophobic core of the protein, not in the loop (Figure 9). Therefore, the redistribution of surface charges, which drives the closer association of the loop and core at pH 3, somehow promotes a loss of side-chain mobility in the core. In search of a mechanism to explain this response, we surmise that the partial collapse of the binding loop may be partially responsible for the increased rigidity of the core at pH 3.

Differences in Energetic Terms. To further assess the effects of structural movement of the loop in terms of energetics, we have compared several intraprotein interaction

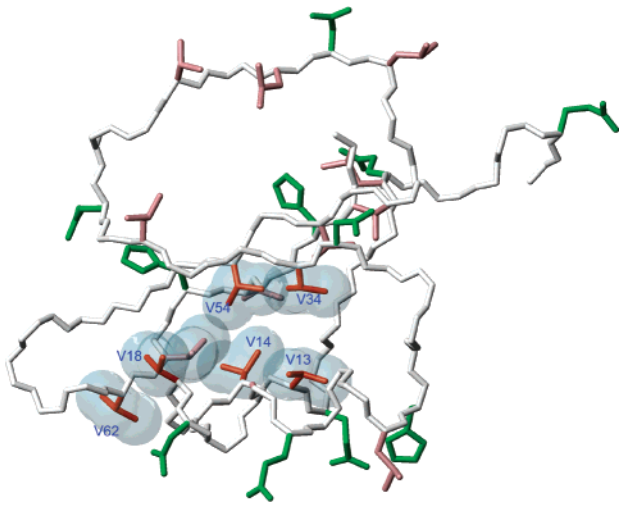

FIGURE 9: Structure of eglin c, shown with titratable side chains (green) and side chains containing methyl groups (pink and orange). The side chains that experience significant changes of order parameters when the pH is lowered to 3 are shown in orange, along with their VDW surfaces.

Table 1: Energy Components Calculated on the Basis of the Dynamics Simulations at Two pH Values (in kilocalories per mole)[a]

	E_{cova}	E_{VDW}	E_{ele}	E_{pack}
pH 3	992 ± 18	−115 ± 11	−1218 ± 39	877 ± 19
pH 7	986 ± 18	−101 ± 12	−1646 ± 112	885 ± 19

[a] The covalent energy E_{cova} is the sum of bond angle, torsion, and improper torsion energies. E_{VDW} is the van der Waals (Lennard-Jones) energy. E_{ele} is the internal electrostatic energy. E_{pack} is the sum of E_{cova} and E_{VDW} as defined.

terms: the covalent energy (bond angle, dihedral, and improper dihedral), the van der Waals energy (the 6−12 interactions), the intramolecular electrostatic energy, and the packing energy defined by Vorobjev and Hermans (*77*, *78*), as computed in the MD simulations (Table 1). Relative to that at pH 7, the electrostatic interaction energy at pH 3 is higher (disfavored), which is expected for a particle with a large net charge. Normally, this energy will be offset by a more favorable solvation energy (*77*, *78*). Of particular note, the packing energy and van der Waals energy are both lower at pH 3, indicating a better-packed structure (on the average), which may also be attributed to the collapse of the loop. Correlations between packing density and dynamical properties have been proposed (*79*), and are discussed below.

DISCUSSION

Most proteins are destabilized as the pH is lowered significantly below neutrality. Under such acidic conditions, protonation of negatively charged side-chain groups disrupts intramolecular hydrogen bonds and electrostatic interactions, thereby destabilizing the protein and ultimately causing denaturation. Loss of these space-directed interactions allows the protein to seek compensatory stabilization from interactions with solvent molecules, possibly through different side chain orientations. Intuition also tells us that destabilized proteins should be more flexible since “stable” proteins are typically structured and “unstable” proteins (i.e., unfolded) have a great deal of disorder. This type of reasoning leads to a prediction that residues gain flexibility as proteins are increasingly protonated or, more generally, destabilized.

Table 2: Structure-Based Components of Conformational Entropies of the Dynamics Simulations at Two pH Values (in calories per mole per kelvin)[a]

	$S_{l,t}$	$S_{c,t}$	$S_{lc,t}$
pH 3	540.29	2065.87	2489.31
pH 7	584.37	2076.00	2526.86

[a] $S_{l,t}$ is the total conformational entropy of the loop region. $S_{c,t}$ is the total conformational entropy of the core region. $S_{lc,t}$ is the total conformational entropy of the core and loop region.

Indeed, this is often observed, as exemplified by acid-induced molten globule states (*7*). However, our results here are at odds with this general expectation. The concurrent destabilization and rigidification of eglin c at low pH has been established from chemical denaturation, NMR spin relaxation, and molecular dynamics simulations. As will be discussed, a combination of approaches helps us to begin to understand this unexpected and complicated behavior, as well as clarify the distinction between stability and conformational rigidity in proteins.

Rigidity and Entropy. Compared with the subtle changes in overall structure and backbone dynamics, eglin c gains considerable rigidity at the side-chain level at low pH. Since model-free order parameters characterize the sampling of phase space, the increased methyl group order parameters indicate that eglin c has lower conformational entropy (*80*, *81*) at low pH. Realizing that angular motions measured as order parameters only count for part of the total conformational entropy, we have calculated the contribution to the conformational entropy from the simulation results. As indicated, for both the loop and the central core of the protein, the pH 3 state always has a lower conformational entropy than the pH 7 state, which provides further evidence for the rigidification of eglin c at low pH (Table 2). One may further decompose the conformational entropy into backbone and side-chain components from the simulations, and this analysis reflects the same trends (data not shown). In summary, both S^2 and conformational entropy analyses consistently reveal a picture of eglin c undergoing rigidification at the side-chain level at pH 3.

Origin of Increased Rigidity. The data and analysis presented here are insufficient for determining with certainty the physical basis for rigidification on the picosecond to nanosecond time scale under destabilizing pH conditions. However, the MD simulations have provided a starting point for mechanistic insights. Although both experimental and simulation data indicate that no major conformational changes occur in the protein, from the MD simulations it appears that the loop region, with greater inherent flexibility, experiences some degree of conformational change, and this may be linked to the observed increase in rigidity at pH 3. The N-terminal segment (first seven residues) is found to be very flexible under both pH conditions and shows few interactions with the core part of the protein. It is therefore unlikely that the N-terminus makes an important contribution to the observed difference. In contrast, the binding loop has moderate flexibility, as evident from ^{15}N relaxation (Figures 4 and 5) and also makes a number of contacts with the protein core (Figure 7). With these considerations, it appears that any significant structural change that might be related to the increase in rigidity is likely to reside in the binding loop.

As calculated from the simulations, the radius of gyration of the protein (excluding the N-terminus) at pH 7 is larger than that at pH 3 by a small but definite amount of 0.3 Å (Figure 8). This is consistent with an overall protein structure and/or shape that is not perturbed much between the two pH states. However, the mass-weighted rms distances between the loop and the center of mass of the core part of the protein (difference of 1.0 Å) demonstrate clear structural variation between pH 3 and 7 for the loop region, primarily in the positioning of the loop relative to the core part of the protein (Figure 8). The loop is closer to the core of the protein at pH 3 because the hydrogen bond between Arg53 and Asp46 (at pH 7) is broken due to neutralization of the Asp46 side chain. In the absence of the interaction between Asp46 and Arg53, the loop is free to move toward the core of the protein, making the protein more compact and rigid, on the average, as shown in the apparent increase in the number of van der Waals packing interactions (Table 1). In conjunction with improved packing interactions, the largest losses of picosecond to nanosecond motion occur in the protein's side chains within the hydrophobic core. It should be mentioned that due to the transient nature of some of these hydrogen bonds and packing interactions, as well as the semiflexible nature of the loop, these observations would be difficult to make from X-ray or NMR experimental data, and highlight the utility of MD simulations.

On the basis of our observations that at pH 3 the protein side chains are more rigid and its structure is better-packed (on average), it is tempting to implicate an inverse, causal relationship between the quality of packing (or packing density) and internal mobility. Such correlations have been proposed from analysis of high-resolution X-ray structures (*79*) and seem entirely reasonable. However, an analysis of a database of NMR-derived S_{axis}^2 values with regard to local packing densities (of methyl groups) has shown that there is little correlation between them (*70*). The apparent discrepancy of these two results may become smaller after considering that the majority of X-ray structures were analyzed (*79*) under cryogenic temperatures (85−120 K). As fast side-chain fluctuations, reflected in S_{axis}^2 values, have been shown to quench at temperatures of <200 K (*82*, *83*), the inverse relation of packing density and flexibility observed in the X-ray structures corresponds in large part to fluctuations considerably smaller in amplitude than those reported by S_{axis}^2. On the other hand, the current availability of NMR-derived side-chain dynamical parameters (e.g., S_{axis}^2) is still limited, leaving the question open. Much of the relationship between packing and picosecond to nanosecond fluctuations, as reported from NMR spin relaxation, remains to be elucidated, and correlated motions are suspected to be an important consideration (*70*). With the increasing availability of high-resolution structures, dynamics data, and high-precision simulation tools, more definitive conclusions may be drawn in the future.

Although a full mechanistic explanation for the picosecond to nanosecond rigidification remains unclear, the increased rigidity of eglin c at low pH is likely to stem, in part, from coupling to the apparent collapse of the loop toward the core of the protein. One can also envision other possible contributing interactions; for instance, neutralization of Asp and Glu side chains disrupts the intramolecular hydrogen bonding and salt bridge interactions. As a result, the side chains of Arg

and Lys can reorient, the charged end to interact with solvent and the hydrophobic part of these side chains to interact with other hydrophobic groups. Analysis of the simulations results shows that for pH 7 and 3 states, the solvent accessible surfaces (SAS) are 828 and 860 Å^2 for the terminal charged groups of Arg and Lys and 1864 and 1795 Å^2 for hydrophobic groups, respectively, which includes the hydrophobic part of Arg and Lys residues. The SAS of the terminal groups of Arg and Lys is larger at pH 3, and the SAS of all hydrophobic groups is smaller at pH 3, showing simultaneously increased solvent exposure of the charged side chains and burial of hydrophobic groups under acidic pH conditions. The increased level of burial of hydrophobic groups may decrease the accessible free volume of side-chain methyl groups and thus add to the increased rigidity at acidic pH. Therefore, the SAS areas appear to support the hypothesis that perturbation of electrostatic interactions can contribute to the rigidification process through side-chain reorientations. However, there is no simple way to quantitatively differentiate the contribution of this mechanism and that from the collapse of the loop.

One may argue that the increase in rigidity at low pH will destabilize the native state through a reduction of the conformational entropy and, in doing so in parallel with the observed decrease of unfolding enthalpy (*28*), violate the classical observation of "enthalpy−entropy compensation" (*84*−*86*). However, several considerations prevent a rigorous argument for this. The spin relaxation and simulation studies carried out in this study are limited to picosecond to nanosecond motions. Other longer time scale motions could compensate for the entropic loss on the picosecond to nanosecond time scale. As of yet, we have not observed appreciable levels of microsecond to millisecond motion by NMR in more than a few residues, nor have we observed significant changes in them (work in progress). In addition, true enthalpy−entropy compensation addresses the entire system, which includes all intraprotein, protein−water, and water−water interactions. The conformational entropies raised from bond vector reorientations only correspond to part of all intraprotein interactions, a relatively small fraction of the total interaction scheme.

Difference between Rigidity and Stability. From the results presented here, it is evident that a distinction should be drawn between stability and rigidity, which are often viewed as equivalent or parallel properties, or as two aspects of a single property. This usage is particularly common in discussions of protein folding and unfolding processes. From studies on the relationship between conformational flexibility and activity in thermophilic enzymes, it has been proposed that increased conformational rigidity is required to stabilize thermophilic enzymes against thermal denaturation (*84*−*87*). Interestingly, observations similar to our results have also been reported for extremophilic proteins (*8*), with the exception that those observations were made with respect to motions on the millisecond time scale. A strength of the spin relaxation approach used here is that the microscopic dynamical features are directly obtained from the data, as opposed to amide hydrogen exchange (*8*), in which dynamics are inferred but there is no direct motional or entropic information. These studies help in showing that the specific behavior and degree of correlation between flexibility and rigidity are dependent on the specific protein, as well as the motional time scales that are investigated.

The results presented here demonstrate that the loss of native-like stability can be accompanied by an *increase* in rigidity. Protein *stability* involves interplay between the macromolecule and its solvent, with a free energy landscape modulated by enthalpic and entropic contributions from both players. Protein *rigidity* is solely a matter of the molecule's own conformational entropy over a range of time scales, without regard for the surroundings. In terms of energetics, rigidity can arise either from a favored interaction such as better packing, in our case, or from a disfavored interaction such as a highly stressed system, which needs other interactions to recompense the stress. In terms of entropy, rigidity only indicates narrowing of phase space, or decreasing of conformational entropy for the structural part investigated. In the absence of further information describing in detail the origin of the structural rigidity and compensatory behaviors of the molecular system, no reliable conclusion about stability can be drawn from studies of rigidity, and *vice versa*, at least on the picosecond to nanosecond time scale. As such, more care should be taken in distinguishing these properties, and direct connections between them should not be assumed.

Comparison with Other Studies of pH-Dependent Dynamics. The effect of pH on protein dynamics has been studied previously using NMR (*9*, *11*, *14*−*16*, *88*), tryptophan fluorescence (*10*), and MD simulations (*74*). Collectively, these studies show that as the pH is significantly removed from neutrality, the protein is destabilized while concomitantly gaining various degrees of flexibility, consistent with common expectation. From those studies, it appears that pH destabilization affects protein dynamics in a way that can be predicted from the general picture of chemical or heat denaturation; that is, as the protein moves closer to the denatured state energetically, it becomes more disordered. It should be noted that pH destabilization differs from chemical or heat destabilization in that protons bind (or dissociate) progressively to discrete side chains, as opposed to nonspecific heat or denaturant access to all or most sites in the protein, which makes the study of pH titration uniquely significant to protein structure, dynamics, and energetics. In a study most similar to that presented here, Kasimova et al. (*16*) compared picosecond to nanosecond backbone flexibility in human growth hormone at pH 7.0 and 2.7. They found, through ^{15}N spin relaxation, that while the structure of human growth hormone remained native, the backbone became more flexible at low pH. Here, pH-dependent dynamics have been characterized site specifically at both the backbone and side-chain levels to reveal a different, novel behavior. Neither the global tumbling time nor the order parameters of individual N−H bond vectors change significantly between the two pH states, suggesting that the conformation *and* backbone NH dynamics of structured parts of the protein are largely unaffected by the pH shift. Thus, the novel result here, through the example of eglin c, is that increased motion on the picosecond to nanosecond (or other) time scale does not necessarily accompany acid-induced destabilization, and in fact, the protein can become more rigid, as reported most effectively by changes in side-chain mobility.

ACKNOWLEDGMENT

We thank Dr. Marshall Edgell, Fang Yi, and Dorothy Sims for providing the eglin c plasmid and for kind assistance on protein expression, purification, and stability studies. We also thank Sagar Khare and Emilie Lopes-Fernandes for interpretation of additional NMR experiments. We thank the scientific computing support at the University of North Carolina at Chapel Hill for providing this computing resource.

SUPPORTING INFORMATION AVAILABLE

Comparison of the backbone N−H and side-chain methyl axial order parameters from NMR experiments and MD simulations. This material is available free of charge via the Internet at http://pubs.acs.org.

REFERENCES

1. Zipp, A., and Kauzmann, W. (1973) Pressure denaturation of metmyoglobin, *Biochemistry 12*, 4217−4228.
2. Frauenfelder, H., Petsko, G. A., and Tsernoglou, D. (1979) Temperature-dependent X-ray diffraction as a probe of protein structural dynamics, *Nature 280*, 558−563.
3. Brooks, C. L., III, Karplus, M., and Pettitt, B. M. (1988) *Proteins: a theoretical perspective of dynamics, structure, and thermodynamics*, Vol. LXXI, John Wiley & Sons, New York.
4. Timasheff, S. N. (1993) The control of protein stability and association by weak interactions with water: how do solvents affect these processes, *Annu. Rev. Biophys. Biomol. Struct. 22*, 67−97.
5. Wang, A., Robertson, A. D., and Bolen, D. W. (1995) Effects of a naturally occurring compatible osmolyte on the internal dynamics of ribonuclease A, *Biochemistry 34*, 15096−15104.
6. Fersht, A. (1998) *Structure and mechanism in protein science*, W. H. Freeman and Co., New York.
7. Ptitsyn, O. (1996) How molten is the molten globule? *Nat. Struct. Biol. 3*, 488−490.
8. Hernandez, G., Jenney, F. E., Adams, M. W. W., and LeMaster, D. M. (2000) Millisecond time scale conformational flexibility in a hyperthermophile protein at ambient temperature, *Proc. Natl. Acad. Sci. U.S.A. 97*, 3166−3170.
9. Brutscher, B., Brüschweiler, R., and Ernst, R. R. (1997) Backbone dynamics and structural characterization of the partially folded A state of ubiquitin by ^{1}H, ^{13}C, and ^{15}N nuclear magnetic resonance spectroscopy, *Biochemistry 36*, 13043−13053.
10. D'Auria, S., Rossi, M., Nucci, R., Irace, G., and Bismuto, E. (1997) Perturbation of conformational dynamics, enzymatic activity, and thermostability of β-Glycosidase from archaeon *Sulfolobus solfataricus* by pH and sodium dodecyl sulfate detergent, *Proteins: Struct., Funct., Genet. 27*, 71−79.
11. Kim, S., Brackenf, C., and Baum, J. (1999) Characterization of millisecond time-scale dynamics in the molten globule state of α-Lactalbumin by NMR, *J. Mol. Biol. 294*, 551−560.
12. Arrington, C. B., and Robertson, A. D. (2000) Microsecond to minute dynamics revealed by EX1-type hydrogen exchange at nearly every backbone hydrogen bond in a native protein, *J. Mol. Biol. 296*, 1307−1317.
13. Sari, N., Alexander, P., Bryan, P. N., and Orban, J. (2000) Structure and dynamics of an acid-denatured protein G mutant, *Biochemistry 39*, 965−977.
14. Kipping, M., Zarnt, T., Kiessig, S., Reimer, U., Fischer, G., and Bayer, P. (2001) Increased backbone flexibility in threonine^{45}-phosphorylated Hirudin upon pH change, *Biochemistry 40*, 7957−7963.
15. Yao, J., Chung, J., Eliezer, D., Wright, P. E., and Dyson, H. J. (2001) NMR structural and dynamic characterization of the acid-unfolded state of apomyoglobin provides insights into the early events in protein folding, *Biochemistry 40*, 3561−3571.
16. Kasimova, M. R., Kristensen, S. M., Howe, P. W. A., Christensen, T., Matthiesen, F., Petersen, J., Sørensen, H. H., and Led, J. J. (2002) NMR studies of the backbone flexibility and structure of human growth hormone: a comparison of high and low pH conformations, *J. Mol. Biol. 318*, 679−695.
17. Kay, L. E., Torchia, D. A., and Bax, A. (1989) Backbone dynamics of proteins as studied by ^{15}N inverse detected heteronuclear NMR spectroscopy: application to staphylococcal nuclease, *Biochemistry 28*, 8972−8979.
18. Palmer, A. G., Kroenke, C. D., and Loria, J. P. (2001) NMR methods for quantifying microsecond-to-millisecond motions in biological macromolecules, *Methods Enzymol. 339*, 204−238.
19. Muhandiram, D. R., Yamazaki, T., Sykes, B. D., and Kay, L. E. (1995) Measurement of ^{2}H T_1 and $T_{1\rho}$ relaxation times in uniformly ^{13}C-labeled and fractionally ^{2}H-labeled proteins in solution, *J. Am. Chem. Soc. 117*, 11536−11544.
20. Yang, D., Mittermaier, A., Mok, Y.-K., and Kay, L. E. (1998) A study of protein side-chain dynamics from new ^{2}H auto-correlation and ^{13}C cross-correlation NMR experiments: application to the N-terminal SH3 domain from drk, *J. Mol. Biol. 276*, 939−954.
21. Lee, A. L., Flynn, P. F., and Wand, A. J. (1999) Comparison of ^{2}H and ^{13}C NMR relaxation techniques for the study of protein methyl group dynamics in solution, *J. Am. Chem. Soc. 121*, 2891−2902.
22. Case, D. A. (2002) Molecular dynamics and NMR spin relaxation in proteins, *Acc. Chem. Res. 35*, 325−331.
23. Brüschweiler, R. (2003) New approaches to the dynamic interpretation and prediction of NMR relaxation data from proteins, *Curr. Opin. Struct. Biol. 13*, 175−183.
24. Seemuller, U., Fritz, H., and Eulitz, M. (1981) Eglin-elastase cathepsin-G inhibitor from leeches, *Methods Enzymol. 80*, 804−816.
25. Bode, W., Papamokos, E., and Musil, D. (1987) The high-resolution X-ray crystal structure of the complex formed between subtilisin *Carlsberg* and eglin c, an elastase inhibitor from the leech *Hirudo medicinalis*. structural analysis, subtilisin structure and interface geometry, *Eur. J. Biochem. 166*, 673−692.
26. Hipler, K., Priestle, J. P., Rahuel, J., and Grütter, M. G. (1992) X-ray crystal structure of the serine proteinase inhibitor eglin c at 1.95 Å resolution, *FEBS Lett. 309*, 139−145.
27. Hyberts, S. G., Goldberg, M. S., Havel, T. F., and Wagner, G. (1992) The solution structure of eglin c based on measurement of many NOEs and coupling constants and its comparison with X-ray structures, *Protein Sci. 1*, 736−751.
28. Bae, S.-J., and Sturtevant, J. M. (1995) Thermodynamics of the thermal unfolding of eglin c in the presence and absence of guanidinium chloride, *Biophys. Chem. 55*, 247−252.
29. Peng, J. W., and Wagner, G. (1992) Mapping of the spectral densities of nitrogen−hydrogen bond motions in Eglin c using heteronuclear relaxation experiments, *Biochemistry 31*, 8571−8586.
30. Peng, J. W., and Wagner, G. (1995) Frequency spectrum of NH bonds in eglin c from spectral density mapping at multiple fields, *Biochemistry 34*, 16733−16752.
31. Yi, F., Sims, D. A., Pielak, G. J., and Edgell, M. H. (2003) Testing hypotheses about determinants of protein structure with high-precision, high-throughput stability measurements and statistical modeling, *Biochemistry 42*, 7594−7603.
32. Stites, W. E., Byrne, M. P., Aviv, J., Kaplan, M., and Curtis, P. M. (1995) Instrumentation for automated determination of protein stability, *Anal. Biochem. 227*, 112−122.
33. Edgell, M. H., Sims, D. A., Pielak, G. J., and Yi, F. (2003) High-precision, high-throughput stability determinations facilitated by robotics and a semi-automated titrating fluorometer, *Biochemistry 42*, 7587−7593.
34. Santoro, M. M., and Bolen, D. W. (1988) Unfolding free energy changes determined by the linear extrapolation method. 1. Unfolding of phenylmethanesulfonyl α-chymotrypsin using different denaturants, *Biochemistry 27*, 8063−8068.
35. Delaglio, F., Grzesiek, S., Vuister, G. W., Zhu, G., Pfeifer, J., and Bax, A. (1995) NMRPipe: a multidimensional spectral processing system based on UNIX pipes, *J. Biomol. NMR 6*, 277−293.
36. Johnson, B. A., and Blevins, R. A. (1994) NMRVIEW: a computer program for the visualization and analysis of NMR data, *J. Biomol. NMR 4*, 603−614.
37. Goddard, T. D., and Kneller, D. G. (2002) *Sparky*, University of California, San Francisco.
38. Muhandiram, D. R., and Kay, L. E. (1994) Gradient-enhanced triple-resonance three-dimensional NMR experiments with improved sensitivity, *J. Magn. Reson., Ser. A 103*, 203−216.
39. Kay, L. E., Xu, G.-Y., Singer, A. U., Muhandiram, D. R., and Forman-Kay, J. D. (1993) A gradient-enhanced HCCH-TOCSY

experiment for recording side-chain ^{1}H and ^{13}C correlations in H_2O samples of proteins, *J. Magn. Reson., Ser. B 101*, 333−337.
40. Uhrín, D., Uhrínová, S., Leadbeater, C., Nairn, J., Price, N. C., and Barlow, P. N. (2000) 3D $HCCH_3$-TOCSY for resonance assignment of methyl-containing side chains in ^{13}C-labeled proteins, *J. Magn. Reson. 142*, 288−293.
41. Neri, D., Szyperski, T., Otting, G., Senn, H., and Wüthrich, K. (1989) Stereospecific nuclear magnetic resonance assignments of the methyl groups of valine and leucine in the DNA-binding domain of the 434 repressor by biosynthetically directed fractional ^{13}C labeling, *Biochemistry 28*, 7510−7516.
42. Yamazaki, T., Muhandiram, R., and Kay, L. E. (1994) NMR experiments for the measurement of carbon relaxation properties in highly enriched, uniformly ^{13}C,^{15}N-labeled proteins: application to $^{13}C\alpha$ carbons, *J. Am. Chem. Soc. 116*, 8266−8278.
43. Pelton, J. G., Torchia, D. A., Meadow, N. D., and Roseman, S. (1993) Tautomeric states of the active-site histidines of phosphorylated and unphosphorylated III^{Glc}, a signal-transducing protein from *Escherichia coli*, using two-dimensional heteronuclear NMR techniques, *Protein Sci. 2*, 543−558.
44. Yamazaki, T., Forman-Kay, J. D., and Kay, L. E. (1993) Two-dimensional NMR experiments for correlating $^{13}C\beta$ and $^{1}H\delta/\epsilon$ chemical shifts of aromatic residues in ^{13}C-labeled proteins via scalar couplings, *J. Am. Chem. Soc. 115*, 11054−11055.
45. Farrow, N. A., Muhandiram, R., Singer, A. U., Pascal, S. M., Kay, C. M., Gish, G., Shoelson, S. E., Pawson, T., Forman-Kay, J. D., and Kay, L. E. (1994) Backbone dynamics of a free and a phosphopeptide-complexed Src homology 2 domain studied by ^{15}N NMR relaxation, *Biochemistry 33*, 5984−6003.
46. Peng, J. W., and Wagner, G. (1994) Investigation of protein motions via relaxation measurements, *Methods Enzymol. 239*, 563−596.
47. Peng, J. W., Thanabal, V., and Wagner, G. (1991) 2D heteronuclear NMR measurements of spin−lattice relaxation times in the rotating frame of X nuclei in heteronuclear HX spin systems, *J. Magn. Reson. 94*, 82−100.
48. Lipari, G., and Szabo, A. (1982) Model-free approach to the interpretation of nuclear magnetic resonance relaxation in macromolecules. 1. Theory and range of validity, *J. Am. Chem. Soc. 104*, 4546−4559.
49. Dellwo, M. J., and Wand, A. J. (1989) Model-independent and model-dependent analysis of the global and internal dynamics of cyclosporin A, *J. Am. Chem. Soc. 111*, 4571−4578.
50. Barbato, G., Ikura, M., Kay, L. E., Pastor, R. W., and Bax, A. (1992) Backbone dynamics of calmodulin studied by ^{15}N relaxation using inverse detected two-dimensional NMR spectroscopy: the central helix is flexible, *Biochemistry 31*, 5269−5278.
51. Tjandra, N., Kuboniwa, H., Ren, H., and Bax, A. (1995) Rotational dynamics of calcium-free calmodulin studied by ^{15}N-NMR relaxation measurements, *Eur. J. Biochem. 230*, 1014−1024.
52. Lipari, G., and Szabo, A. (1982) Model-free approach to the interpretation of nuclear magnetic resonance relaxation in macromolecules. 2. Analysis of experimental results, *J. Am. Chem. Soc. 104*, 4559−4570.
53. Mann, G., Yun, R. H., Nyland, L., Prins, J., Board, J., and Hermans, J. (2002) in *Computational Methods for Macromolecules: Challenges and Applications* (Schlick, T., and Gan, H. H., Eds.) pp 129−145, Springer, New York.
54. MacKerell, A. D., Jr., Bashford, D., Bellott, M., Dunbrack, R. L., Jr., Evanseck, J. D., Field, M. J., Fischer, S., Gao, J., Guo, H., Ha, S., Joseph-McCarthy, D., Kuchnir, L., Kuczera, K., Lau, F. T. K., Mattos, C., Michnick, S., Ngo, T., Nguyen, D. T., Prodhom, B., Reiher, W. E., III, Roux, B., Schlenkrich, M., Smith, J. C., Stote, R., Straub, J., Watanabe, M., Wiorkiewicz-Kuczera, J., Yin, D., and Karplus, M. (1998) All-atom empirical potential for molecular modeling and dynamics studies of proteins, *J. Phys. Chem. B 102*, 3586−3616.
55. Jorgensen, W. L., Chandrasekhar, J., Madura, J. D., Impey, R. W., and Klein, M. L. (1983) Comparison of simple potential functions for simulating liquid water, *J. Chem. Phys. 79*, 926−935.
56. Tuckerman, M. E., Berne, B. J., and Martyna, G. J. (1992) Reversible multiple time scale molecular dynamics, *J. Chem. Phys. 97*, 1990−2001.
57. Schlick, T., Skeel, R. D., Brünger, A. T., Kalé, L. V., Board, J. A., Hermans, J., and Schulten, K. (1999) Algorithmic challenges in computational molecular biophysics, *J. Comput. Phys. 151*, 9−48.
58. Ryckaert, J. P., Ciccotti, G., and Berendsen, H. J. C. (1977) Numerical integration of the Cartesian equations of motion of a system with constraints: molecular dynamics of *n*-alkanes, *J. Comput. Phys. 23*, 327−341.
59. Darden, T. A., York, D. M., and Pedersen, L. G. (1993) Particle mesh Ewald: an N.log(N) method for Ewald sums in large systems, *J. Chem. Phys. 98*, 10089−10092.
60. Berendsen, H. J. C., Postma, J. P. M., van Gunsteren, W. F., DiNola, A., and Haak, J. R. (1984) Molecular dynamics with coupling to an external bath, *J. Chem. Phys. 81*, 3684−3690.
61. Smith, P. E., Schaik, R. C. v., Szyperski, T., Wüthrich, K., and van Gunsteren, W. F. (1995) Internal mobility of the basic pancreatic trypsin inhibitor in solution: A comparison of NMR spin relaxation measurements and molecular dynamics simulations, *J. Mol. Biol. 246*, 356−365.
62. Chatfield, D. C., Szabo, A., and Brooks, B. R. (1998) Molecular dynamics of staphylococcal nuclease: comparison of simulation with ^{15}N and ^{13}C NMR relaxation data, *J. Am. Chem. Soc. 120*, 5301−5311.
63. Karplus, M., and Kushick, J. N. (1981) Methods for estimating the configurational entropy of macromolecules, *Macromolecules 14*, 325−332.
64. Di Nola, A., Berendsen, H. J. C., and Edholm, O. (1984) Free-energy determination of polypeptide conformations generated by molecular dynamics, *Macromolecules 17*, 2044−2050.
65. Schlitter, J. (1993) Estimation of absolute and relative entropies of macromolecules using the covariance matrix, *Chem. Phys. Lett. 215*, 617−621.
66. Schäfer, H., Mark, A. E., and van Gunsteren, W. F. (2000) Absolute entropies from molecular dynamics simulation trajectories, *J. Chem. Phys. 113*, 7809−7817.
67. Andricioaei, I., and Karplus, M. (2001) On the calculation of entropy from covariance matrices of the atomic fluctuations, *J. Chem. Phys. 115*, 6289−6292.
68. Schurr, J. M., Babcock, H. P., and Fujimoto, B. S. (1994) A test of the Model-Free formulas. Effects of anisotropic rotational diffusion and dimerization, *J. Magn. Reson., Ser. B 105*, 211−224.
69. Lee, L. K., Rance, M., Chazin, W. J., and Palmer, A. G. (1997) Rotational diffusion anisotropy of proteins from simultaneous analysis of ^{15}N and $^{13}C^{\alpha}$ nuclear spin relaxation, *J. Biomol. NMR 9*, 287−298.
70. Mittermaier, A., Kay, L. E., and Forman-Kay, J. D. (1999) Analysis of deuterium relaxation-derived methyl axis order parameters and correlation with local structure, *J. Biomol. NMR 13*, 181−195.
71. Wand, A. J. (2001) Dynamic activation of protein function: A view emerging from NMR spectroscopy, *Nat. Struct. Biol. 8*, 926−931.
72. Lienin, S. F., Bremi, T., Brutscher, B., Brüschweiler, R., and Ernst, R. R. (1998) Anisotropic intramolecular backbone dynamics of ubiquitin characterized by NMR relaxation and MD computer simulation, *J. Am. Chem. Soc. 120*, 9870−9879.
73. Pfeiffer, S., Fushman, D., and Cowburn, D. (2001) Simulated and NMR-derived backbone dynamics of a protein with significant flexibility: A comparison of spectral densities for the βARK1 PH domain, *J. Am. Chem. Soc. 123*, 3021−3036.
74. Prompers, J. J., Scheurer, C., and Brüschweiler, R. (2001) Characterization of NMR relaxation-active motions of a partially folded A-state analogue of ubiquitin, *J. Mol. Biol. 305*, 1085−1097.
75. Price, D. J., and Brooks, C. L., III (2002) Modern protein force fields behave comparably in molecular dynamics simulations, *J. Comput. Chem. 23*, 1045−1056.
76. Prabhu, N. V., Lee, A. L., Wand, A. J., and Sharp, K. A. (2003) Dynamics and entropy of a calmodulin-peptide complex studied by NMR and molecular dynamics, *Biochemistry 42*, 562−570.
77. Vorobjev, Y. N., Almagro, J. A., and Hermans, J. (1998) Discrimination between native and intentionally misfolded conformations of proteins: ES/IS, a new method for calculating conformational free energy that uses both dynamics simulations with explicit solvent and a continuum solvent model, *Proteins: Struct., Funct., Genet. 32*, 399−413.
78. Vorobjev, Y. N., and Hermans, J. (2001) Free energies of protein decoys provide insight into determinants of protein stability, *Protein Sci. 10*, 2498−2506.
79. Halle, B. (2002) Flexibility and packing in proteins, *Proc. Natl. Acad. Sci. U.S.A. 99*, 1274−1279.

80. Li, Z., Raychaudhuri, S., and Wand, A. J. (1996) Insights into the local residual entropy of proteins provided by NMR relaxation, *Protein Sci. 5*, 2647−2650.
81. Yang, D., and Kay, L. E. (1996) Contributions to conformational entropy arising from bond vector fluctuations measured from NMR-derived order parameters: application to protein folding, *J. Mol. Biol. 263*, 369−382.
82. Doster, W., Cusack, S., and Petry, W. (1989) Dynamical transition of myoglobin revealed by inelastic neutron scattering, *Nature 337*, 754−756.
83. Lee, A. L., and Wand, A. J. (2001) Microscopic origins of entropy, heat capacity and the glass transition in proteins, *Nature 411*, 501−504.
84. Lumry, R., and Rajender, S. (1970) Enthalpy−entropy compensation phenomena in water solutions of proteins and small molecules: a ubiquitous property of water, *Biopolymers 9*, 1125−1227.
85. Cooper, A., Johnson, C. M., Lakey, J. H., and Nöllmann, M. (2001) Heat does not come in different colours: entropy−enthalpy compensation, free energy windows, quantum confinement, pressure perturbation calorimetry, solvation and the multiple causes of heat capacity effects in biomolecular interactions, *Biophys. Chem. 93*, 215−230.
86. Sharp, K. (2001) Entropy−enthalpy compensation: Fact or artifact? *Protein Sci. 10*, 661−667.
87. Závodszky, P., Kardos, J., Svingor, Á., and Petsko, G. A. (1998) Adjustment of conformational flexibility is a key event in the thermal adaptation of proteins, *Proc. Natl. Acad. Sci. U.S.A. 95*, 7406−7411.
88. Song, J., Michael Laskowski, J., Qasim, M. A., and Markley, J. L. (2003) Two conformational states of *Turkey Ovomucoid* third domain at low pH: Three-dimensional structures, internal dynamics, and interconversion kinetics and thermodynamics, *Biochemistry 42*, 6380−6391.
89. Li, A. and Daggett, V. (1995) Investigation of the solution structure of chymotrypsin inhibitor 2 using molecular dynamics: comparison to X-ray crystallographic and NMR data. *Protein Eng. 8*, 1117−28.

BI035015Z